Applied Catalysis B: Environmental 310 (2022) 121343

Contents lists available at ScienceDirect

Applied Catalysis B: Environmental

journal homepage: www.elsevier.com/locate/apcatb

Highly efficient uranium extraction by a piezo catalytic reduction-oxidation process

Yawen Cai [a,b], Yifeng Zhang [a], Zhimin Lv [a], Shuo Zhang [a], Feixue Gao [a], Ming Fang [a,*], Mingguang Kong [c], Peisheng Liu [d], Xiaoli Tan [a,*], Baowei Hu [b], Xiangke Wang [a,b,**]

[a] College of Environmental Science and Engineering, North China Electric Power University, Beijing 102206, PR China
[b] School of Life Science, Shaoxing University, Shaoxing 312000, PR China
[c] Institute of Solid State Physics, Chinese Academy of Sciences, Hefei 230031, PR China
[d] School of Information Science and Technology, Nantong University, Nantong 226019, PR China

ARTICLE INFO

Keywords:
Piezo catalysis
Adsorption-reduction-peroxidation reaction
U(VI)
$(UO_2)O_2{\cdot}2H_2O$
Zn_2SnO_4/SnO_2

ABSTRACT

In this work, a highly efficient uranium extraction method from water by the piezo catalytic reduction-oxidation process is reported by utilizing a hollow cubic shaped Zn_2SnO_4/SnO_2 as piezo catalyst. The electrons and holes in Zn_2SnO_4/SnO_2 are separated efficiently under the irradiation of ultrasound. After that, some of the piezo electrons reduce the adsorbed U(VI) to UO_2, the others react with soluble oxygen to form H_2O_2, and oxidize UO_2 to generate $(UO_2)O_2{\bullet}2H_2O$, which could be efficiently separated from the solution. U(VI) piezo catalytic extraction rate could reach ~ 90% under the irradiation of ultrasonic waves (40 kHz, 120 W) within 5 h and only decreased by ~ 3% after four cycles. The present work advances piezo catalysis as a new route for uranium extraction from water, which may be applied in the extraction or removal of U(VI) in the U-containing wastewaters, providing new opportunities for resource-saving and environmental enhancement.

1. Introduction

Environment and energy are two momentous issues related to the living and daily production of the human being. Greatly expanded usage of nuclear power has alleviated the dependence on fossil fuels and reduced the emissions of greenhouse gas. Uranium is the key element for nuclear fuel due to its high energy density. However, the mining and utilization of U(VI) may produce a large amount of U-containing water, which may cause severe pollution and waste of resources if discharged without treatment. On the other hand, the uranium element (U(VI)) exists in water (such as sea and Salt Lake) with reserves of about 500 ~ 1000 times that in the land [1,2]. Therefore, the extraction and recycling of uranium-contained water have become one of the central issues for energy saving and environmental treatment. Many methods are usually used to extract soluble uranium from wastewater, such as precipitation [3], organic solvent extraction [4], adsorption [5,6], photocatalysis [7,8], electrocatalysis [9] etc. However, all of them suffer various problems in a real application, such as a large amount of reagent consumption and easily generating secondary waste [7], etc. Therefore, developing brand-new ways to enrich U(VI) from water is urgent, and is also full of challenges.

Piezo catalysis is a recently developed technology aiming at pollution treatment by utilizing piezoelectric nanomaterials. The driving force of piezo catalysis mainly comes from charge transfer and separation triggered by the structure deformation under the irradiation of ultrasound [10]. Theoretically, the piezo catalysis could utilize mechanical energy harvested from various natural activities, such as wind, flowing water, rain drop, tide, and ocean waves. It has been proved to be effective in water splitting, organic pollutants degradation, and bacterial disinfection [11–15]. The reported research mainly targeted the oxidation process of organic pollutants (such as dyes and antibiotics) [13,16–20], and only a few studies have been involved in water splitting and the reduction of heavy metals. Especially the latter, as far as we know, only Cr(VI) is reported to be reduced by piezo reduction until now [21,22]. This should be ascribed to the large quantities of generated •OH and $\bullet O_2^-$ in the ultrasonic process, which mainly act as oxidizers while the chemical reaction [11] and make it difficult to achieve the reduction process. To date, abundant materials

* Corresponding authors.
** Corresponding author at: College of Environmental Science and Engineering, North China Electric Power University, Beijing 102206, PR China.
E-mail addresses: mfang@ncepu.edu.cn (M. Fang), xltan@ncepu.edu.cn (X. Tan), xkwang@ncepu.edu.cn (X. Wang).

https://doi.org/10.1016/j.apcatb.2022.121343
Received 2 February 2022; Received in revised form 18 March 2022; Accepted 20 March 2022
Available online 24 March 2022

have shown the piezoelectric effect. However, the enhancement of piezo catalysis by composite materials is seldom reported. Most of the reported research on piezo catalysis is based on the single component nanomaterial. However, the composition may increase the separation rate of electrons and holes of the nanomaterials and thus lead to the increase of catalytic efficacy.

As an attractive n-type dual semiconducting oxide, the anti-spinel structured endows Zn_2SnO_4 with good piezoelectric property, thermodynamic stability, superior acid-base resistance property, high electrical conductivity, and high electron diffusivity [23]. In our previous publication, SnO_2 was found to have a good affinity with U(VI) as well as high conductivity [24]. Therefore in this work, strong piezo catalytic activity for uranium extraction was realized in the presence of a novel and preeminent piezo catalyst, Zn_2SnO_4/SnO_2 (ZSO/SO) hollow nanocube. The U(VI) piezo catalytic extraction rate could reach ~ 90% under the irradiation of ultrasonic waves (40 kHz, 120 W) within 5 h. Comprehensive experiments were carried out to study the mechanism of piezo catalytic removal of U(VI), which was ascribed to a complex process of adsorption-reduction-peroxidation to form $(UO_2)O_2$•2 H_2O. This stable uranium peroxide is of great importance as intermediate compound both at the front-end and back-end of the nuclear fuel cycle. Through this method, the U(VI) in wastewater is expected to be extracted by piezo catalysis, at the same time, our work demonstrates that the piezoelectric materials have full potential for heavy metal ions extraction as well as polluted water treatment by harvesting mechanical energy from the environment.

2. Experimental sections

2.1. Chemicals and materials

Zinc nitrate hexahydrate ($Zn(NO_3)_2{\cdot}6H_2O$, 99%), tin chloride pentahydrate ($SnCl_4{\cdot}5H_2O$, 99.0%), zinc oxide (ZnO, 99.8% metals basis, 50 ± 10 nm), and stannic oxide (SnO_2, 99.5%) were purchased from Shanghai Aladdin Bio-Chem Technology Co., LTD (Shanghai, China). Hexamethylenetetramine (HMT, 99%) was obtained from Xiya Chem. Co., LTD (Shandong, China). Hexadecyl trimethyl ammonium bromide (CTAB), sodium hydroxide (NaOH), and nitric acid (HNO_3) were supplied by Shanghai Macklin Biochemical Co., LTD (Shanghai, China). All the other reagents were of analytical grades and used as received without further purification.

2.2. Synthesis of ZSO/SO 160–240 nanocomposites

All the reagents were of analytical purity and used without further purification. ZnO nanorods were firstly synthesized by a one-pot low-temperature reflux method [25] (see details in supporting information) and used as starting zinc source for the synthesis of Zn_2SnO_4/SnO_2 (ZSO/SO) nanocomposites. In brief, 219 mg of cetyltrimethylammonium bromide (CTAB), 158 mg of $SnCl_4{\cdot}5H_2O$, and 11 mg of ZnO rods were successively added into 30 mL of 0.15 M NaOH solution to form a uniform reaction solution. The synthesis was performed in a 50 mL Teflon-lined stainless-steel autoclave, severally maintained at 160, 180, 200, 220, and 240 °C for 12 h and then naturally cooled down to ambient temperature in the oven. The resulting white precipitates were isolated by suction filtration, thoroughly rinsed with deionized water and ethanol. The products were harvested and dried for 4 h at 90 °C. The sample was named ZSO/SO T, where T denotes the temperature of the hydrothermal reaction.

2.3. Synthesis of pure SnO_2 and Zn_2SnO_4

SnO_2 was prepared via a similar hydrothermal method as ZSO/SO without adding ZnO. Specifically, 219 mg CTAB and 158 mg $SnCl_4{\cdot}5H_2O$ were added into 30 mL of 0.15 M NaOH solution, then it was reacted at 220 °C for 12 h. The resultant was filtered, thoroughly washed with deionized water and ethanol before being dried in an oven. Zn_2SnO_4 was prepared by heating the mixture of ZnO and SnO_2 powders in a muffle furnace by segmentation calcination. Specifically, 0.03 mol (2.44 g) ZnO and 0.012 mol (1.81 g) SnO_2 powders were fully mixed and ground for 30 min in an agate mortar. The mixture was then evenly spread in a quartz boat and thermally treated in muffle furnace at 400 °C for 300 min. After that, the furnace cooled down to room temperature, and the obtained product was collected and ground for another 30 min. The powder was then collected and filled in the quartz boat and annealed in the muffle furnace at 1000 °C for 5 h. Finally, 1.0 g of the calcined product was soaked in 100 mL 0.1 M HNO_3 for 2 h to remove the unreacted ZnO to obtain pure Zn_2SnO_4.

2.4. Characterizations

All samples were characterized by X-ray diffraction (XRD) with a Rigaku SmartLab SE diffractometer using Cu Kα (λ = 1.5406 nm) and operating at 40 kV and 40 mA. FTIR spectra were recorded on a Shimadzu IRTracer-100 Fourier transform spectrometer. The Brunauer-Emmett-Teller (BET) specific surface areas of the materials were detected by HONYEO TriStar II nitrogen adsorption apparatus. Thermogravimetric measurements were analyzed on a thermal analyzer (NETZSCH STA 449F3 Jupiter thermal analyzer) under N_2 atmosphere. Zeta potentials at different pH values were measured on Malvern Zetasizer Nano ZS90. UV–vis diffuse reflection spectra (DRS) were determined on a SHIMADZU UV-2700 UV-Vis spectrophotometer with $BaSO_4$ as the reference. Scanning electron microscopy (SEM) images were observed with a JEOL JSM-6700 F instrument. Transmission electron microscopy (TEM) and High-resolution transmission electron microscopy (HRTEM) images were taken on a JEOL JEM-2100HR field-emission electron microscope attaching by energy dispersive spectra (EDS) mapping and selective area electron diffraction (SAED) accessories. X-ray photoelectron spectra (XPS) were investigated on a ThermoFischer Escalab 250Xi electron spectrometer using Al Kα irradiation ($h\nu$ = 1486.7 eV). Photoluminescence (PL) measurement was achieved from a LS-55 fluorescence spectrophotometer (PerkinElmer, UK) irradiated by the light with wavelength of 220 nm. The piezo response force microscopy (PFM) and scanning Kelvin probe force microscopy (KPFM) measurements were carried out using an atomic force microscopy (AFM, Bruker MultiMode 8, USA). The sample powders were pressed on a conductive silicon wafer substrate for measurements. The localized piezoelectric hysteresis loops were recorded under a ± 9.9 V reversal applied field, and surface potential measurement was characterized with an applied voltage of 10 V.

2.5. Electrochemical experiments

Mott-Schottky (M-S) curves, transient current curves, and electrochemical impedance spectra (EIS) were measured on a CHI660E electrochemical workstation (Shanghai Chenhua Instrument Co., Ltd), based on a three-electrode system (an Ag/AgCl reference electrode, a Pt sheet auxiliary electrode, and the glassy carbon electrode working electrode) in 0.5 M Na_2SO_4 aqueous electrolyte. The M-S measurement was conducted by using an impedance-potential model with a voltage range of − 1.0 ~ 1.0 V and at a frequency of 1000 Hz. The transient piezo-current response was measured under the irradiation of an ultrasonic wave (28 kHz, 50 W). The EIS test was performed at a frequency range between 1 × 10^{-2} and 2 × 10^4 Hz and an amplitude of 5 mV. For the working electrode, 20 μL of 2 mg/mL sample dispersion and 10 μL of 0.5% Nafion ethanol solution were successively cast onto the surface of cleaned glassy carbon electrode (GCE) and dried naturally for hours.

2.6. Piezoelectric catalysis activity measurement

In all the piezo catalytic experiments, 50 mg catalyst powder was dispersed in 50 mL of 50 mg/L U(VI) solution in a glass tube. Without

special instructions, the mixture was stirred for 4.5 h to minimum the influence of adsorption on the piezo catalytic process, then the piezo catalytic experiment was carried out using a homemade ultrasonic machine at a frequency of 40 kHz with the ultrasonic power of 120 W at 20 °C in dark. The influence of coexisted cations on U(VI) removal was investigated by adding $M(NO_3^-)_n$ (0.05 mol/L, M = K^+, Na^+, and Mg^{2+}) and anions of NaX (0.05 mol/L, X = NO_3^-, CO_3^{2-}, and HPO_4^{2-}) into the catalytic reaction system at pH = 3.50. $AgNO_3$ (1 mmol), methanol (10%), dimethyl sulfoxide (DMSO, 1 mmol), and p-benzoquinone (p-BQ, 1 mmol) were used as radical scavengers for electrons (e^-), holes (h^+), •OH, and $•O_2^-$ radicals, respectively. In addition, an experiment with nitrogen purging (N_2, 30 mL/min) in the whole process was conducted to expel the dissolved O_2 from the reaction system. Furthermore, in order to evaluate the recyclability and durability of catalyst, the piezo catalytic experiment was consecutively repeated four cycles of extraction-regeneration by using 0.1 M Na_2CO_3 as eluent. In all experiments, the concentration of residual U(VI) was determined by the UV–vis absorption method monitored at 652 nm using Arsenazo-III as the chromogenic agent.

2.7. Determination of H_2O_2 concentration

The concentration of H_2O_2 was determined by the iodide method. Detailed H_2O_2 quantification experiments were performed as follows [22,26]: 50 mL of 1 mg/mL ZSO/SO 220 suspension and 50 mL ultrapure water (taken as reference) were irradiated by ultrasonic wave after 4.5 h stirring in dark, respectively. 2 mL of the suspension was taken out at regular intervals and filtered by a 0.22 μm filter, and then 4 mL KI (0.1 M) and 100 μL ammonium molybdate tetrahydrate ($H_{32}Mo_7N_6O_{28}$, 0.01 M) solutions were added into 1 mL of the above filtrate. 10 min later, the solution was tested at 351 nm on a UV–vis spectrophotometer (SHIMADZU UV-2700).

3. Results and discussion

3.1. Phase composition analysis and piezo catalytic performance

The phase and crystal structures of the as-obtained catalysts are carefully characterized through XRD analysis (see Fig. 1A). The product synthesized at 160 °C mainly consists of highly crystalized $ZnSn(OH)_6$ (PDF card no. 73–2384) powders. With rising the temperature of the hydrothermal reaction, the peaks of $ZnSn(OH)_6$ evanesced, and those of Zn_2SnO_4 (PDF card no. 73–1725) and SnO_2 (PDF card no. 72–1147) occurred, and dominated in ZSO/SO 180, 200 and 220. For comparison, pure SnO_2 and pure Zn_2SnO_4 nanoparticles were also prepared. More detailed descriptions about phase transition and their morphologies (Fig. S1) are provided in *SI*.

The corresponding piezo catalytic experiments for U(VI) extraction by the obtained samples under the irradiation of 120 W ultrasonic wave are shown in Fig. 1B. It could be seen that the U(VI) concentration in solution is hardly changed without catalyst or the irradiation of ultrasonic wave, indicating the U(VI) is stable at this condition. This result manifests that the piezoelectric material plays an important role, and the influence of sonoluminescence can be excluded in the catalytic process. As all the obtained catalysts were added in, the concentration of U(VI) decreased to different degrees. The pure SnO_2 and pure Zn_2SnO_4 suffer the worst performance. For the sample obtained from different hydrothermal temperatures, the piezo catalytic performance increased as increasing the hydrothermal temperature to 220 °C, then decreased. 75% U(VI) is eliminated by ZSO/SO 220 in solution within 210 min. This could be further demonstrated by utilizing the first-order rate constant (k, the slope of the first-order linear simulation on $\ln(C_0/C)$ vs t, see Fig. S2) in the inset figure of Fig. 1B. The k value of ZSO/SO 220 (0.00712) is approximately 3.60 and 4.68 times those of pure SnO_2 (0.00198) and Zn_2SnO_4 (0.00152), respectively. These results indicate that ZSO/SO 220 possesses superior piezo catalytic activity over the other as-prepared catalysts in U(VI) removal, which is used for further investigation to illuminate the mechanism for the piezo catalytic extraction of U(VI).

3.2. Validation of piezoelectric property of ZSO/SO 220

The piezoresponse force microscopy (PFM) and Kelvin probe force microscopy (KPFM) is used firstly to validate the piezoelectric property of the sample. The PFM topographic, amplitude and phase images of the ZSO/SO 220 nanocubes are shown in Fig. 2(A-C). It can be observed that the sample heights of ZSO/SO 220 fluctuate in the range of − 101.2 ~ 66.6 nm in a randomly selected 10 × 10 μm^2 scanning area (Fig. 2A). Two distinct contrasts are observed in the relative amplitude images (Fig. 2B) and the phase switching signals (Fig. 2C), which clearly show that piezoelectric response is created in ZSO/SO 220 [27,28]. The clear phase contrast between different regions represents the domain with opposite polarization orientation. These piezoelectric domains can also be identified in the amplitude image [27,28]. A well-defined butterfly-shaped displacement-voltage hysteresis response can be seen from Fig. 2D, further confirming the excellent piezoelectricity of ZSO/SO 220 [15,29,30]. An approximately 180° phase difference contrast (from −50° to 130°) in piezoelectric response phase reversal hysteresis loop is presented in Fig. 2E, together with two different color contrast differences (Fig. 2B), validating the switching nature of the domains in the

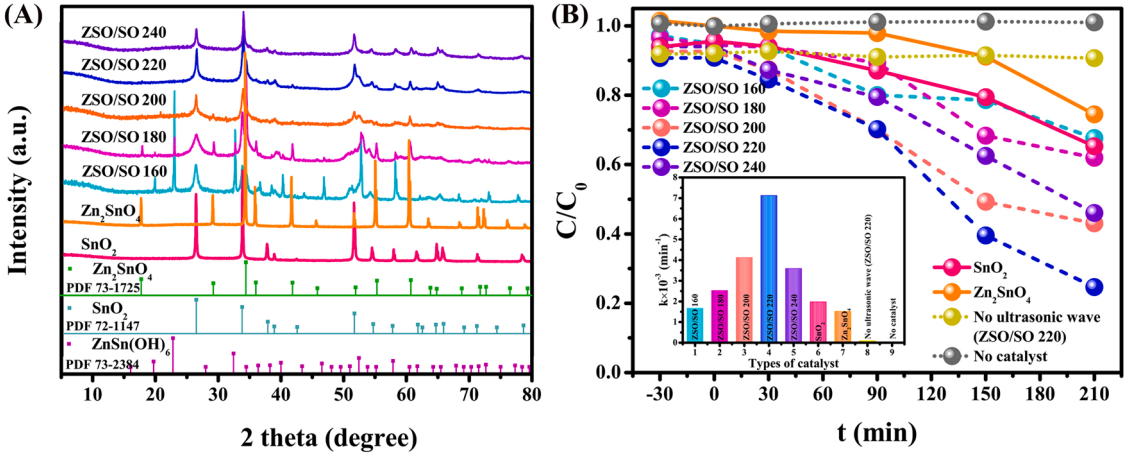

Fig. 1. (A) XRD patterns of ZSO/SO 160–240, SnO_2, and Zn_2SnO_4; (B) The piezo catalytic activities of ZSO/SO 160–240, SnO_2, and Zn_2SnO_4 for U(VI) and the corresponding fitted results of the removal rate constant (inset). m/V= 1.0 g/L, $C_{U(VI)\ initial}$= 50 mg/L, pH ~ 3.50, T = 293 K, and the parameters of ultrasonic wave: 40 kHz, 120 W.

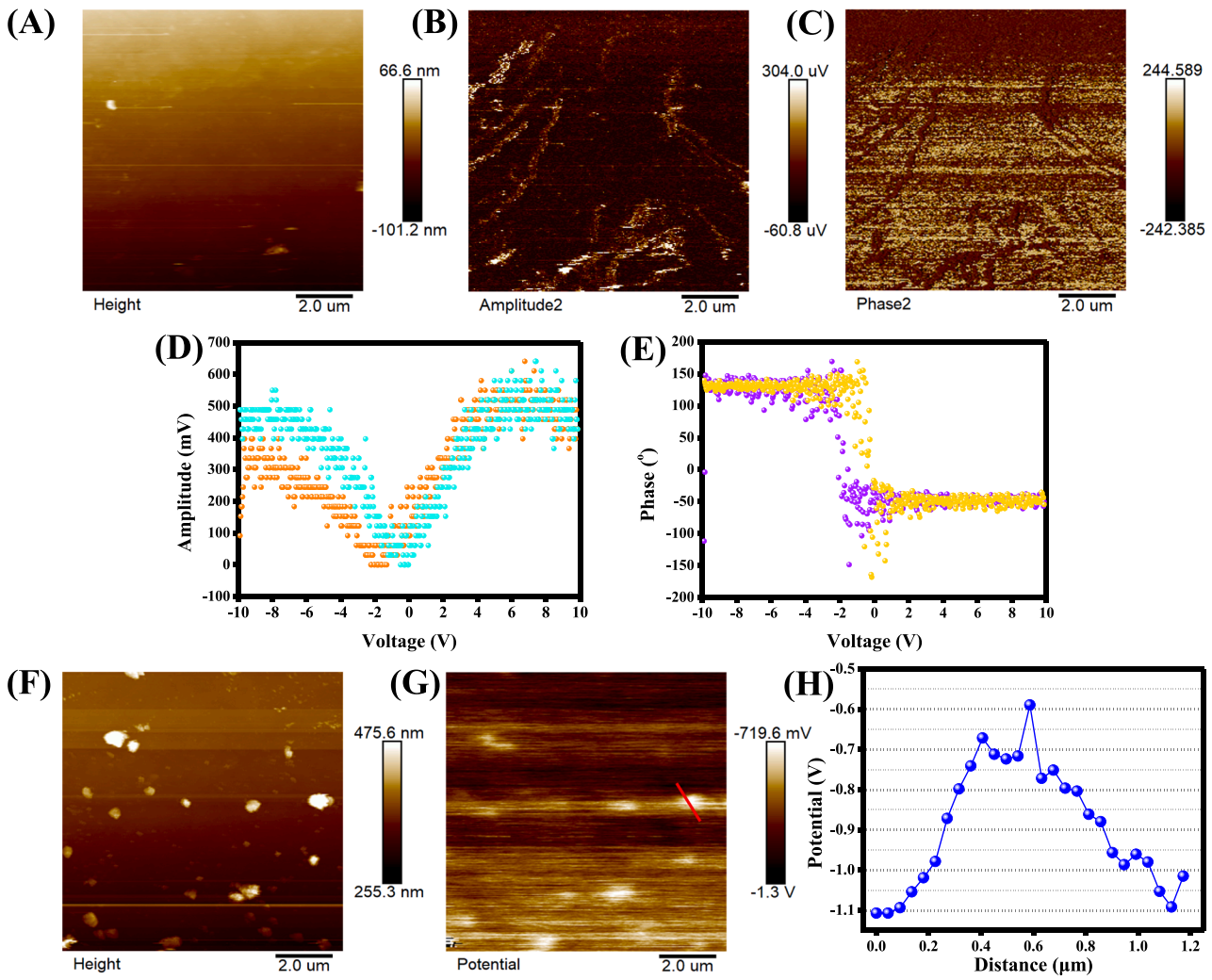

Fig. 2. PFM results of ZSO/SO 220: (A) surface topology, (B) amplitude, (C) phase images, and Local hysteresis loop behavior for the (D) amplitude and (E) phase; and KPFM (F) topography image, (G) the corresponding surface potential image, and (H) the surface potential distribution on the selected line for ZSO/SO 220.

ZSO/SO 220 [29,30]. The KPFM is employed to identify the surface piezoelectric potential by measuring the contact potential difference (CPD) between the tip and the sample. Fig. 2(F-H) displays the surface topography of ZSO/SO 220 and its inhomogeneous surface potential image, and the surface potential distribution on the selected line, respectively. Under the stress of the probe tip, an inward built-in electric field forms inside the ZSO/SO 220, resulting in a negative surface voltage change between − 0.6 and − 1.1 V, proving its eximious piezoelectric property [31,32].

3.3. Characterization and Identification of piezo catalytic products

The above results indicate that the piezoelectric property of ZSO/SO 220 could work in the piezo catalytic extraction of U(VI), thereafter ZSO/SO 220 composites before and after piezo catalysis are further investigated by TEM/EDS to demonstrate whether the uranium is enriched on the sample. Fig. 3 shows hollow nanocube-like morphology with the shell thicknesses in the range of 200 ~ 250 nm by the obvious contrast of the dark edges and the pale center, and the enlarged view on the nanocube shows that it is constructed by lots of nanorods with a diameter of ~ 8 nm. Interestingly, these nanorods are basically stood vertically on the surface of the box. Most importantly, the details of samples before and after piezo catalysis do not show the obvious difference, meaning it is stable in the piezo catalytic process (Figs. 3C and F). It should be noted that after the piezo catalytic experiment, U elements are obviously observed in the EDS mapping (Fig. 4A and B). Further EDS mapping investigation (Fig. 4C-F) clearly shows the similar profiles of Zn, Sn, O, and U elements, indicating U element is homogeneously distributed on the surface of the ZSO/SO 220 hollow nanocube, namely, U is successfully enriched on the surface of the piezo catalyst.

The XPS was used to investigate the elemental valence state of uranium on ZSO/SO 220 after piezo catalysis to reflect the reaction mechanism. From the survey spectrum shown in Fig. 5A, Zn, Sn, O, and U could be observed. Further investigation by the high-resolution spectrum shows well-fitted double peaks at 381.75 and 392.51 eV, which are corresponded to the U 4 $f_{7/2}$ and U 4 $f_{5/2}$ peaks, and indicate the existence of U(VI), without U(IV) (Fig. 5B) [33,34]. Since no reports related to the piezo catalysis of U(VI) can be referenced, the XPS result here indicates that the ultrasonic process is more like an adsorption process rather than a catalytic reaction. However, before the piezo catalytic process begins, the samples have been previously dispersed in ultrasonic irradiation (400 W, 40 kHz) without U(VI) for 15 min to destroy the aggregation as much as possible, and the adsorption-desorption equilibrium is achieved before the ultrasonic irradiation. Therefore, the decrease of U(VI) concentration is far from adsorption. Then what kind of mechanism should be responsible for this process? To find the answer to this question, the phase of the samples after piezo catalysis was investigated by XRD with a scan rate of 2° per min and is shown in Fig. 5C. All the samples retain their characteristic peaks except for several new humps appearing in the curves of ZSO/SO

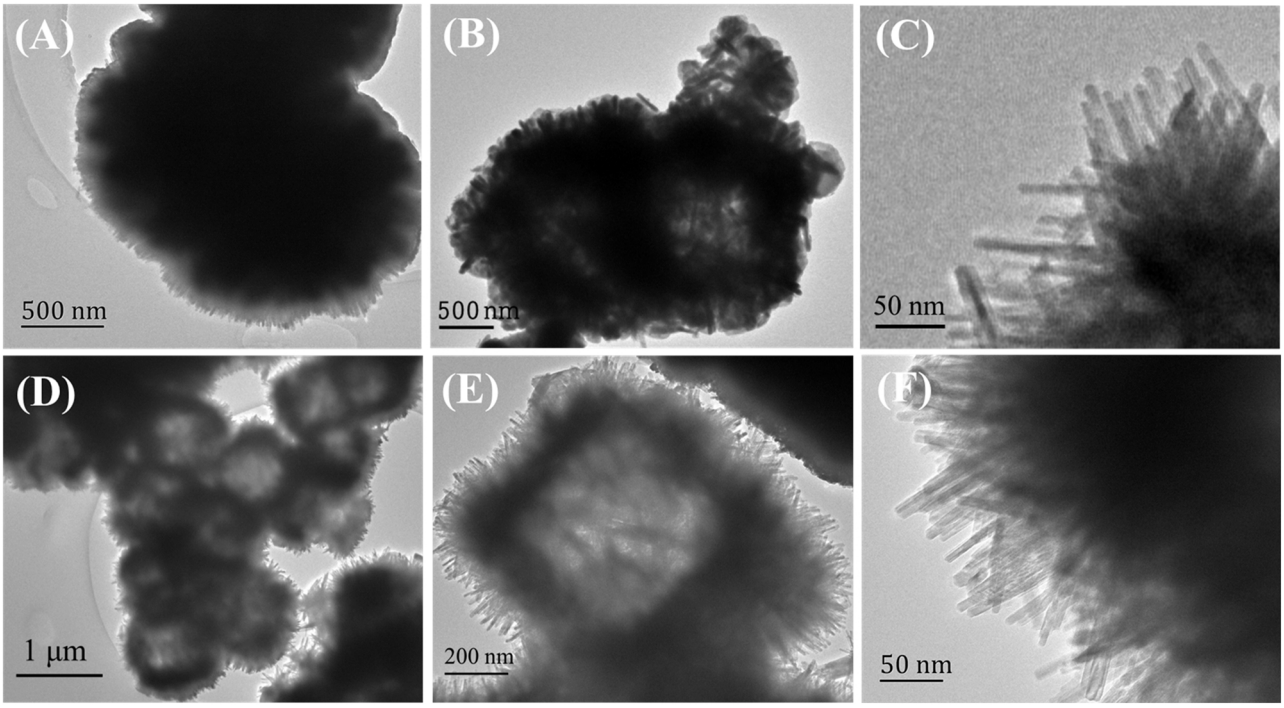

Fig. 3. TEM images of ZSO/SO 220 before (A-C) and after (D-F) catalytic reaction.

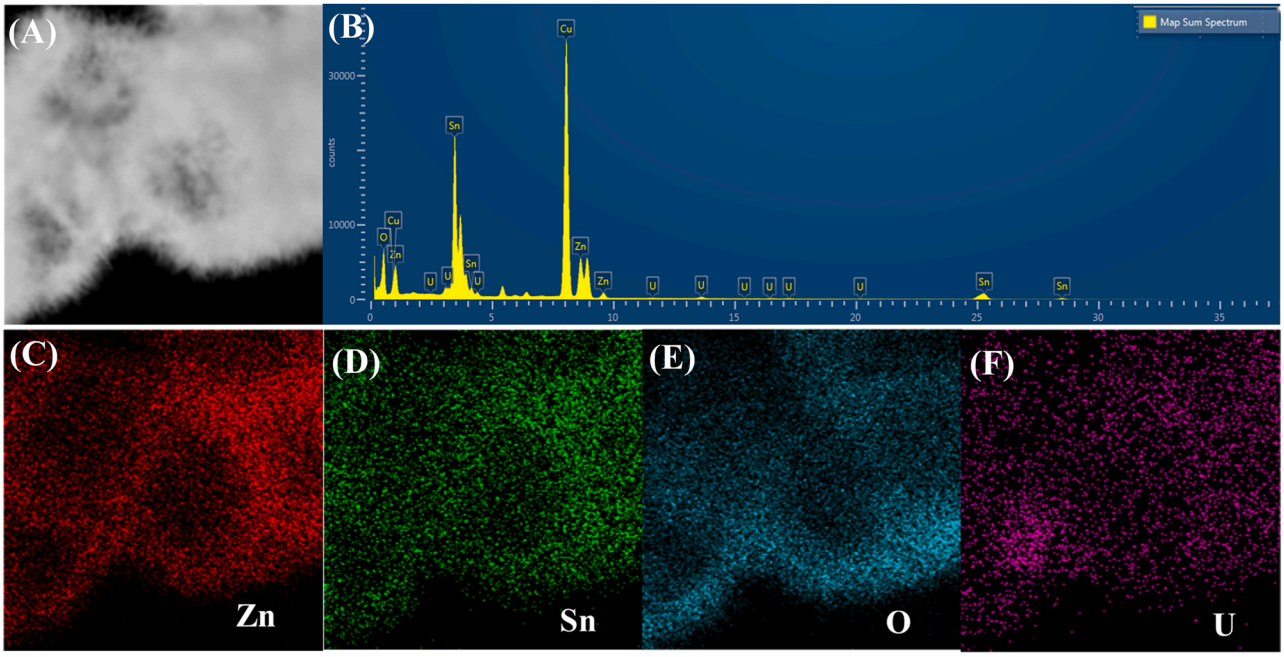

Fig. 4. (A) TEM micrograph, (B) EDS spectrum, and (C-F) the corresponding elemental mapping images (Zn, Sn, O, and U) of ZSO/SO 220 after the catalytic reaction.

180–240, and the position of these peaks is consistent in each sample. These small peaks could also be observed in ZSO/SO 160, SnO_2, and Zn_2SnO_4, but the peak intensities are too weak to be clearly observed without comparison. After careful investigation, these peaks can be indexed to the orthorhombic metastudtite ($(UO_2)O_2{\cdot}2H_2O$, PDF card no. 35-0571), which is known as one of the two naturally existing uranium peroxide species [35].

The identity of the existence of $(UO_2)O_2.2H_2O$ can also be validated by FTIR (Fig. 5D) and HRTEM/SAED (Fig. 5E and F) analysis. The FTIR spectrum of uranium-loaded ZSO/SO 220 under ultrasonication has several characteristic absorption bands: the OH stretching band at approximately 3200–3400 cm^{-1}, the OH bending band (sharp) at 1630 cm^{-1}, and the asymmetric vibration bands of the uranyl group at 928 and 903 cm^{-1}, respectively. The two formers indicate the existence of crystal water or adsorbed water, and the latter indicates the presentation of $(UO_2)O_2.2\ H_2O$ [36], which is also observed in the FTIR spectra of the other samples after piezo catalysis of U(VI) containing water (Figs. S3A and S3B). While these $(UO_2)O_2.2\ H_2O$-related characteristic absorption bands are not observed in the sample without ultrasonic irradiation. The HRTEM image of ZSO/SO 220 after piezo catalysis are

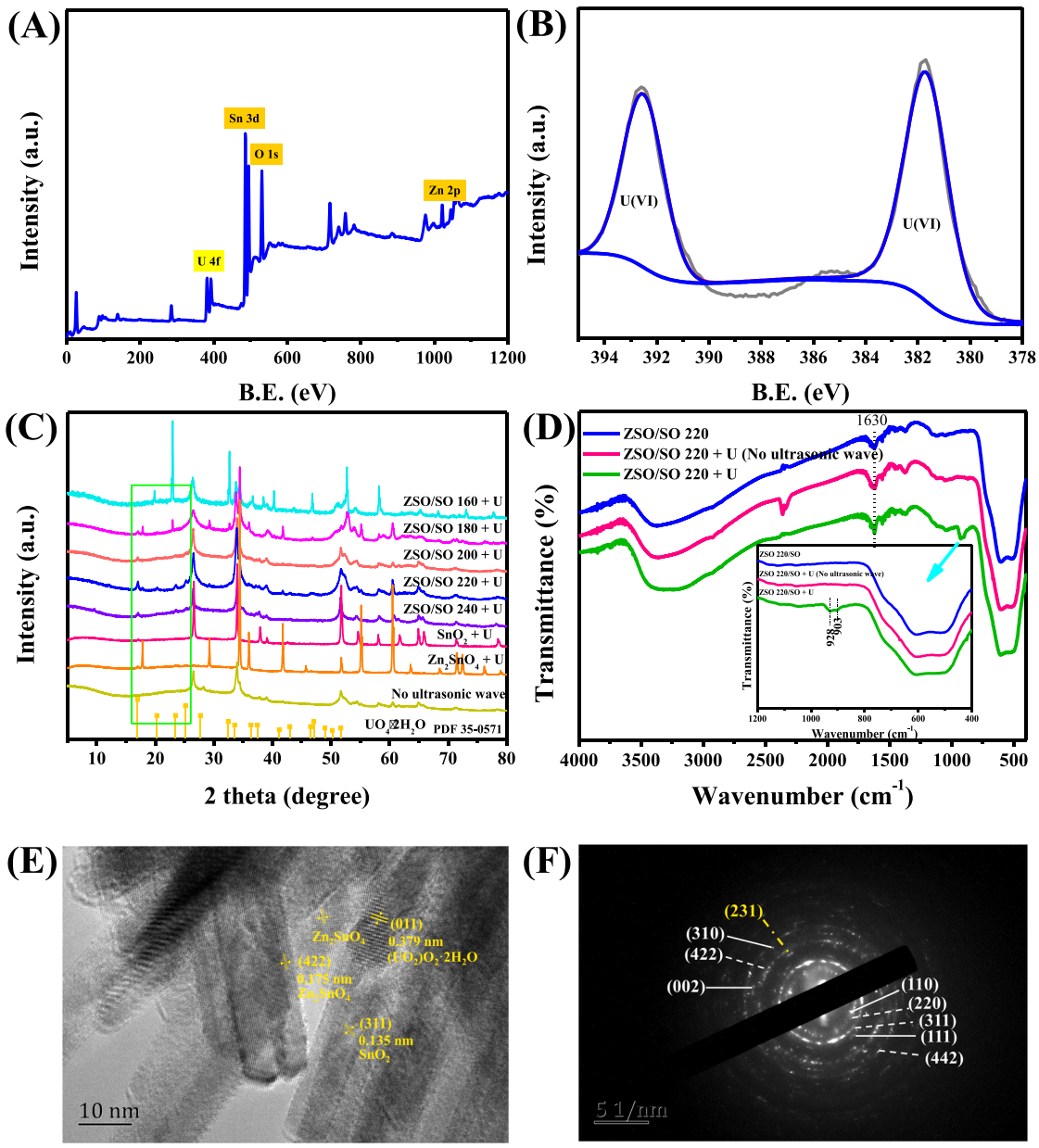

Fig. 5. (A) The survey scan and (B) U 4 f high-resolution XPS spectra, (C) XRD patterns, and (D) FTIR spectra of uranium loaded ZSO/SO 220. m/V= 1.0 g/L, $C_{U(VI)\ initial}$= 50 mg/L, pH= 3.50, T = 293 K, and ultrasonic wave: 40 kHz, 120 W; (E) HRTEM micrograph, and (F) SAED pattern (including the Miller indices for crystallographic planes of SnO_2, Zn_2SnO_4 and $(UO_2)O_2.2\ H_2O$ separately pointed by solid, broken and yellow dash-dot lines) of ZSO/SO 220 after the catalytic reaction.

shown in Fig. 5E, from which clear interplanar spacings of 0.135 nm and 0.175 nm are observed and matched well with the (311) and (422) crystal planes of SnO_2 and Zn_2SnO_4, respectively, indicating the nanocubes of ZSO/SO 220 are a binary complex of SnO_2 and Zn_2SnO_4. Simultaneously, an interplanar spacing of 0.379 nm corresponds to (011) crystal plane of $(UO_2)O_2.2\ H_2O$(s) appeared confirming the formation of uranium peroxides. This could also be observed in the SAED pattern (Fig. 5F), where besides the rings belonging to SnO_2 and Zn_2SnO_4 (See *SI*), an additional diffraction ring could be well-indexed to the (231) plane of $(UO_2)O_2.2\ H_2O$(s).

Based on the above-mentioned experiments, it can be concluded that the U(VI) was captured by forming $(UO_2)O_2.2\ H_2O$. Then a question here is how does the $(UO_2)O_2.2\ H_2O$ form under the effect of ultrasonic wave irradiation? Generally, the first ingredient for the formation of peroxide is the existence or formation of H_2O_2. But H_2O_2 is not added into the system previously, therefore, it must be generated during the ultrasonic irradiation. During the piezo catalysis process in the presence or absence of ZSO/SO 220, the generation of H_2O_2 is measured and found to gradually increase as prolonging the ultrasonic time (Fig. 6A). However, the yield of H_2O_2 under ultrasonic irradiation with ZSO/SO 220 is obviously higher than that without ZSO/SO 220. It should be noted that the U(VI) could not transform into $(UO_2)O_2.2\ H_2O$ in the absence of ZSO/SO 220 as shown in Fig. 1B. That means ZSO/SO 220 plays important role in the U(VI) transformation as well as greatly enhances the production of H_2O_2. Generally, two ways may contribute to the generation of H_2O_2 [21,22],

the reduction of O_2.

$$O_2 + e^- \rightarrow \bullet O_2^- \quad (1)$$

$$\bullet O_2^- + e^- + 2\ H^+ \rightarrow H_2O_2 \quad (2)$$

and the oxidation process of H_2O.

$$2\ H_2O + 2\ h^+ \rightarrow H_2O_2 + 2\ H^+ \quad (3)$$

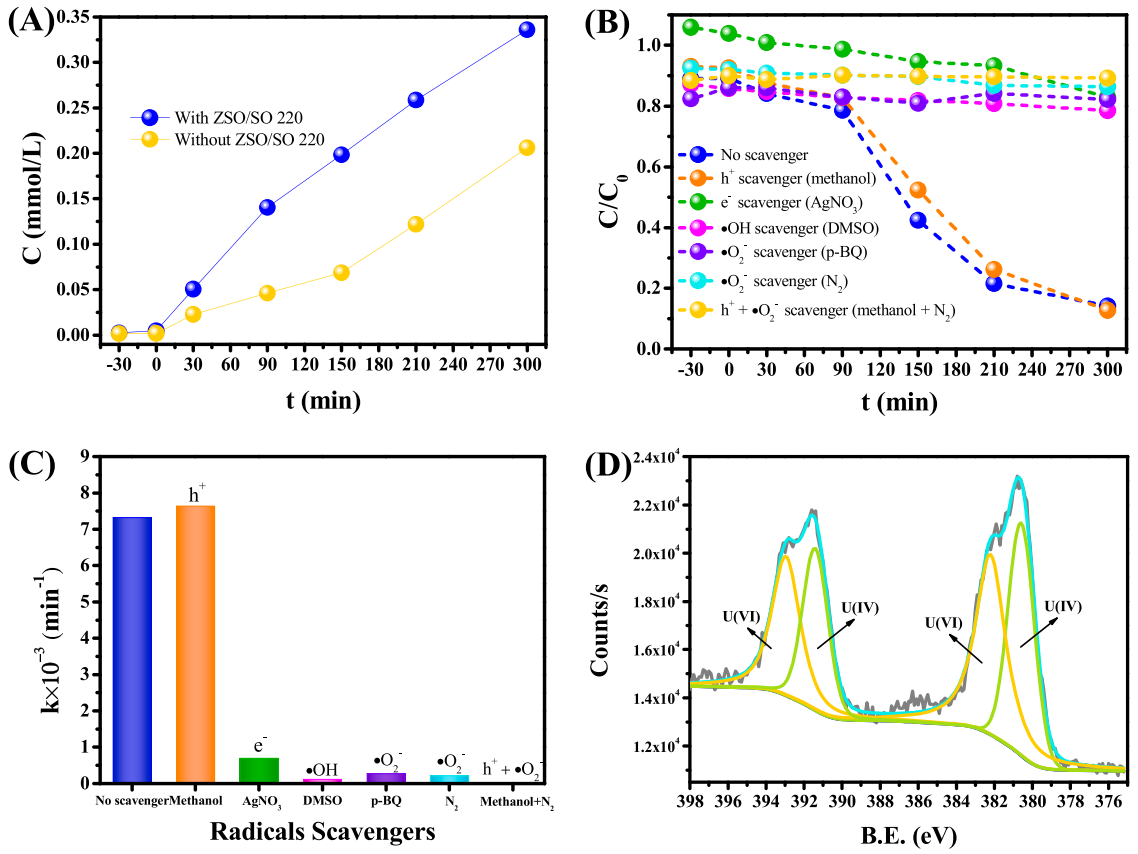

Fig. 6. (A) The generation of H_2O_2 in the presence or absence of ZSO/SO 220 under 40 kHz of 120 W ultrasonic irradiation, m/V= 1.0 g/L, pH= 3.50, T = 293 K; (B) The piezo catalytic experiments with adding different sacrificial agents and (C) the corresponding fitted results of the removal rate constant; (D) U 4 f XPS high-resolution spectrum of ZSO/SO 220 after 60 min ultrasonic irradiation. m/V= 1.0 g/L, $C_{U(VI)\ initial}$= 50 mg/L, T = 293 K, pH= 3.50, and parameters from ultrasonic wave: 40 kHz, 120 W.

The typical difference between these two reactions is whether H^+ is consumed. The pH values before and after the catalytic reaction are measured to be 3.50 and 3.85 in the presence of ZSO/SO 220, and 3.49 and 3.33 in the absence of ZSO/SO 220, respectively. This demonstrates the former is an H^+ consuming process, and the latter is an H^+ generating process. Therefore, it is reasonable to deduce the generation of H_2O_2 with ZSO/SO 220 is mainly by the two-step reduction process of O_2, and that without ZSO/SO 220 is by the oxidation process of H_2O.

To validate this deduction and further demonstrate the mechanism of the piezo catalytic process, different radical scavengers are used in the piezo catalytic processes. As shown in Fig. 6B, C, and S4, when $AgNO_3$, DMSO, or p-BQ is added, the piezo catalytic removal of U(VI) is suppressed greatly by the comparison to that without scavengers, and less than 10% of the U(VI) is removed after 300 min. For the N_2 bubbled experiment, the piezo catalytic activity is almost completely repressed due to the elimination of soluble O_2. These results suggest that the e^-, $•O_2^-$ and •OH play the predominant roles in the piezo catalytic reaction of U(VI). This is because the soluble O_2 molecules are reduced by e^- to generate $•O_2^-$, which then react with e^- and H^+ to form H_2O_2 (Eqs. (1) and (2)) under the irradiation of ultrasonic wave. But for •OH, it could be generated in two ways generally: by the reaction of h^+ with H_2O on the surface of the material (Eq. (4)), or through a reduction reaction of H_2O_2 (Eq. (5)) [20,21].

$$H_2O + h^+ \rightarrow •OH + H^+ \quad (4)$$

$$H_2O_2 + e^- + H^+ \rightarrow •OH + H_2O \quad (5)$$

From Fig. 6C, the piezo catalytic activity is not suppressed by the elimination of h^+, therefore the piezo generated •OH in this work must derive mainly from the reduction of H_2O_2 (Eq. (5)). The elimination of •OH may lead to the consumption of H_2O_2, thus decreasing the transformation of U(VI) to $(UO_2)O_2.2H_2O$. The piezo catalysis is a little promoted as adding methanol, which is because the removal of h^+ may decrease the recombination rate with e^-, thus enhancing the elimination capacity of U(VI) a little.

It should be noted that although H_2O_2 could be formed in water without catalyst (Fig. 6A), no changes in U(VI) concentration are observed under ultrasonic irradiation (Fig. 1B) in this condition, indicating the U(VI) could not react with H_2O_2 directly. The ZSO/SO 220 must have primary responsibility for the transformation from U(VI) to $(UO_2)O_2.2H_2O$. To demonstrate the role of ZSO/SO 220 in the transformation from U(VI) to $(UO_2)O_2.2H_2O$, the kinetics curve of piezo catalysis of ZSO/SO 220 in Fig. 1B is carefully investigated, which shows a clearly reverse *S* shape, indicating the residual U(VI) concentration decreases slowly at first, then decreases fast. This means there must be two or more mechanisms to control the elimination rate of U(VI). To relative accurately identify the different stages in the elimination process, the corresponding time-dependent differential curve is shown in Fig. S5, i.e., the reaction rate vs time curve. The reaction rate increases as prolonging the reaction time, and achieve the maximum at approximately 120 min, after that the reaction rate decreases. Hence, the sample after 60 min piezo catalysis before the inflection point time is collected and analyzed by XPS (Figs. S6 and 6D). Interestingly, besides the peaks belonging to U(VI) at $U4f_{7/2}$ 381.98 eV and $U4f_{5/2}$ 392.79 eV are observed, two new peaks at 380.37 and 391.24 eV are observed (Fig. 6D), which should be ascribed to the $U4f_{7/2}$ and $U4f_{5/2}$ peaks of U (IV) [37–40]. This means in the first stages, a portion of the adsorbed U (VI) is piezo reduced to U(IV) under the irradiation of ultrasound, and it is reasonable to deduce the U(IV) is oxidized to $(UO_2)O_2.2H_2O$ under the action of the continuous generation of H_2O_2.

3.4. Charge transfer efficiency and band structure, and rational piezo catalytic mechanisms

Another question in the above experiments (especially in Fig. 1B) is the piezo catalytic performance of the composites is superior to any single components (SnO_2 and Zn_2SnO_4), which should benefit from highly efficient separation rate and small recombination rate of the piezo induced e^- and h^+ pairs, and could be verified by the photoluminescence (PL) and transient current curves. Fig. S7 exhibits the PL spectra of SnO_2, Zn_2SnO_4, and ZSO/SO 220 in the region of 320–415 nm under the excitation of 220 nm wavelength light. In general, the higher the emission intensity, the faster the recombination of the piezo induced electrons and holes [41]. All three samples show emission peaks centered at around 350 nm, which are related to the transitions near the band edges [42]. The ZSO/SO 220 has the smallest PL intensity among the three samples, indicating the slowest recombination rate of piezo induced electrons and holes in ZSO/SO 220, and thereby the largest population of the piezo induced carriers could be used in the catalytic process. This could also be supported by the transient piezo current response curves (Fig. 7A) [43], where ZSO/SO 220 shows a significantly enhanced transient piezo current response over SnO_2 and Zn_2SnO_4, indicating an improvement in the separation of e^- and h^+ pairs has been achieved in ZSO/SO 220 [44]. These results experimentally provide evidence for the efficient separation of piezo induced carriers, which should be ascribed to the combination of SnO_2 and Zn_2SnO_4.

The optical and electrochemical experiments are also performed to investigate the band matching mechanism between SnO_2 and Zn_2SnO_4. Fig. 7B and C exhibit the room-temperature UV–vis diffuse reflectance spectra (DRS) and the calculated optical band gap patterns of SnO_2 and Zn_2SnO_4, which are measured to be 3.60 and 3.70 eV, respectively, according to the formula proposed by Tauc, Davis, and Mott (see *SI*). Mott-Schottky plots are also recorded to evaluate the flat-band potentials of the samples (Fig. 7D) by extrapolating the linear portion of the plot to the X-axis [45]. From the positive slopes of the obtained plots for SnO_2 and Zn_2SnO_4, the two components are both identified as n-type semiconductors [46]. The flat band potentials (E_{fb}) of SnO_2 and Zn_2SnO_4 are confirmed to be ~ − 0.84 and − 0.69 V (vs. Ag/AgCl), respectively. Generally, for n-type semiconductors, the conduction band potential (E_{CB}) is more negative than the E_{fb} by ~ 0.1 V [15,47]. Thus, the E_{CB} values of SnO_2 and Zn_2SnO_4 are estimated to be − 0.94 V and − 0.79 V, and the E_{VB} values of SnO_2 and Zn_2SnO_4 are evaluated to be 2.66 and 2.91 V, respectively.

Based on the above-mentioned experimental results and analyses, the piezo catalytic mechanism for U(VI) by the ZSO/SO 220 nanocomposite could be proposed as follows (Fig. 8). The U(VI) ions, mainly existing as UO_2^{2+}, are firstly adsorbed onto the surface of ZSO/SO 220 dues to its active adsorption sites. At the same time, under the irradiation of the ultrasonic wave, electrons generated in SnO_2 may transfer to the conduction band of Zn_2SnO_4 due to the conduction band of SnO_2 is a little higher than that of Zn_2SnO_4, and holes generated in Zn_2SnO_4 may transfer to the valence band of SnO_2, thus achieve the aims of highly efficient separation of piezo induced carriers. After that, the adsorbed-UO_2^{2+} may undergo a direct reduction reaction by a portion of piezo generated e^- on the surfaces of catalyst to form U(IV) ($(UO_2(s))$ (Eq. (6)). The rest piezo generated e^- may react with soluble oxygen to form $\bullet O_2^-$, and further produce H_2O_2 by the assistance of H^+, and finally, the $UO_2(s)$ was oxidized to $(UO_2)O_2.2\,H_2O(s)$ by the formed H_2O_2 (Eq. (7)) [48–51].

$$UO_2^{2+} + 2e^- \rightarrow UO_2(s) \quad (6)$$

$$UO_2(s) + 2\,H_2O_2 \rightarrow (UO_2)O_2.2\,H_2O(s) \quad (7)$$

There is a broad literature base to support the reaction of uranium with H_2O_2 in aqueous media proceeding [52,53]. Thereinto, the first recorded discovery of the product of uranium peroxide ($(UO_2)O_2.2\,H_2O$ (s)) is on the surface of UO_2(s) from nuclear waste [50]. The extraction

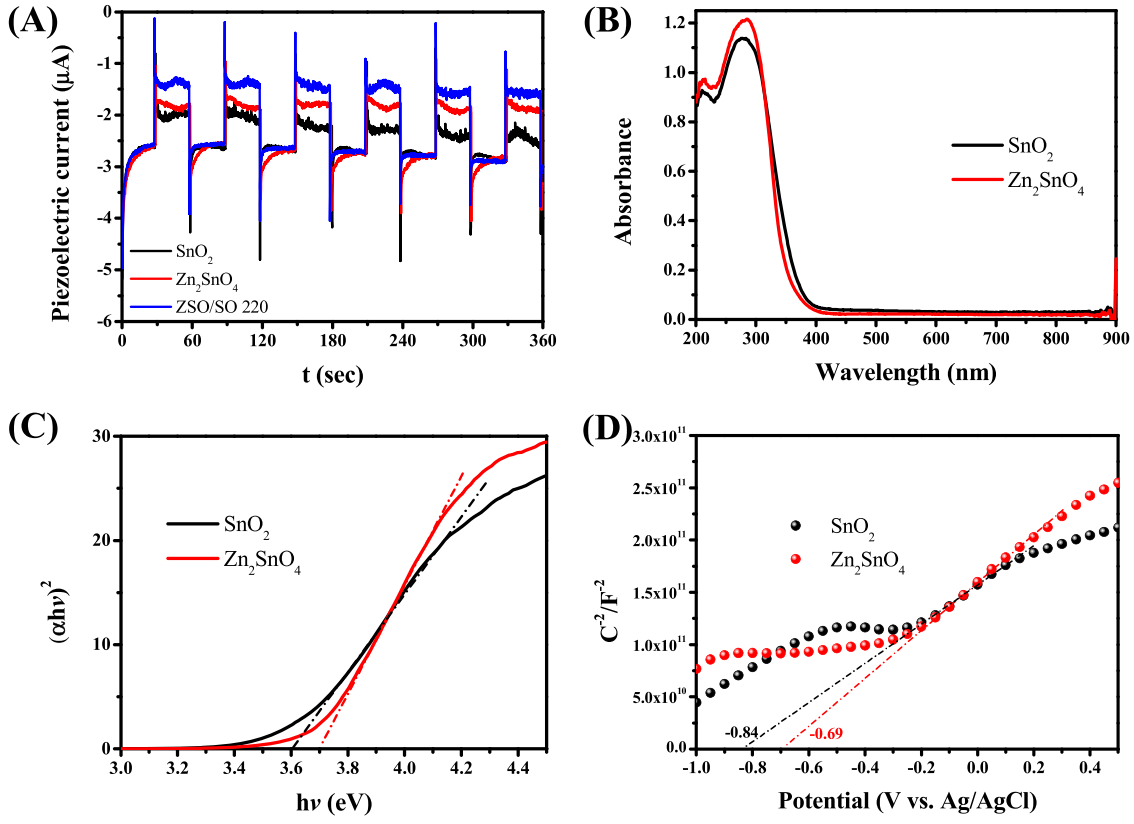

Fig. 7. (A) UV–vis DRS spectra, (B) $(\alpha h\nu)^2$ vs. photon energy curves, and (C) Mott-Schottky plots of SnO_2 and Zn_2SnO_4, (D) transient piezo current response curves of SnO_2, Zn_2SnO_4, and ZSO/SO 220.

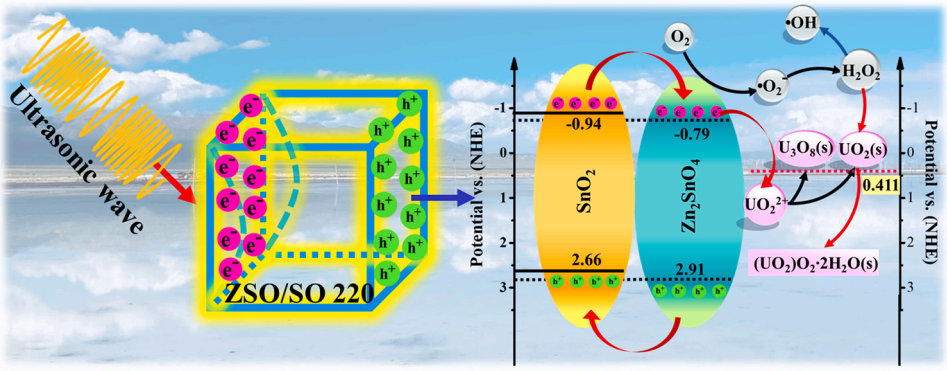

Fig. 8. Schematic energy level diagram of ZSO/SO 220 binary system.

rate of U(VI) is controlled by a three-step process, including the adsorption of U(VI) to the surface of the catalyst, the reduction of U(VI) to U(IV), and the oxidation of U(IV) to U(VI). Within the first 90 min, the amount of generated H_2O_2 is small and the quantity of U(IV) is also small, leading to the unsatisfying catalytic removal rate of U(VI). After that, as the quantities of U(IV) and H_2O_2 increased, the reaction rate continuously increased, and the extraction rate of U(VI) increased either. Thus a reverse S-shaped curve is obtained, which is very different from the previous research [54,55]. Finally, the UO_2(s) may completely transform into $(UO_2)O_2.2H_2O$(s). Furthermore, the property that the $(UO_2)O_2.2\ H_2O$(s) formation decreases the concentration of soluble U (VI) in the system indicates that the metastudtite phase is stable in the presence of H_2O_2 [56]. Nevertheless, either UO_2(s) or $(UO_2)O_2.2H_2O$(s) are insoluble species and could facilitate further immobilization of soluble uranium to ensure a high-efficiently U(VI) extraction from solution.

3.5. *Piezo catalytic uranium extraction performance evaluation under different conditions*

The experimental conditions may have great impact on the performance of the piezo catalysis of U(VI) by ZSO/SO 220 nanocomposites. Therefore, the influences of pH values, temperatures, and ultrasonic powers/frequencies are comprehensively investigated to find the best experimental condition for U(VI) elimination by the piezo catalytic performance of ZSO/SO 220. Fig. 9A and its inset depict the influence of solution pH on the removal of U(VI). At pH 1.5 and 2.5, the removal efficiency is negligible due to the strong competition of H^+ to U(VI) to approach the surface of the catalyst. With further increase in the pH value, the removal efficiency significantly increases, and ~ 90% of 50 ppm U(VI) can be removed within 300 min at pH 3.5 and 4.5. This could be explained by the charged property of the surface of the catalyst. The zeta potential of ZSO/SO 220 declines steadily to zero from pH 1.5–6.72 (Fig. 9B), leading to the weakening of the repulsion between the positively charged surfaces of catalyst and UO_2^{2+}. Moreover, the generated electrons are more readily interact with positively charged protons under acidic conditions, leading to a highly efficient separation rate of electrons and holes [21]. When the pH value is in the range of 5.5–9.5, the most important species of U(VI) is schoepite ($[(UO_2)_8O_2(OH)_{12}]\bullet 12H_2O$, equiv to $UO_3.2.25H_2O$) (Fig. S8), which is typical hydroxide precipitation of hexavalent uranium [57–59]. This can be reflected in the superior removal efficiency of pH 5.5–9.5 to that of pH 1.5–4.5 before ultrasonic irradiation (Fig. 9A). The U(VI) concentration in solution then increases gradually along with the irradiation of ultrasonic waves due to the stripping and crumbling of the formed schoepite. The fragmentized schoepite is too small to be completely separated by centrifugation and filtration. The following acidification step during the uranium concentration measurement may dissolve the hydroxide precipitation, resulting in the increase of U(VI) concentration. However, there is some intriguing difference between pH 5.5 and 7.5, as well as 9.5 during ultrasonic irradiation. At pH 5.5, ~ 30% of U(VI) could be extracted under the effect of ultrasound in the time range from 90 to 300 min, because the formation of H_2O_2 at pH 5.5 is more favorable than at pH 7.5 and 9.5 (Eqs. (1) and (2)). From the calculated results by *Visual MINTEQ ver. 3.0* (Fig. S8), two species of $(UO_2)_3(OH)_5^+$ and UO_2OH^+ mainly exist at this pH region, which can transform to uranium peroxide by the effect of piezo catalysis (Fig. S9A).

The temperature-dependent piezo catalytic experiment of ZSO/SO 220 is further investigated in the temperature range from 278 to 323 K (Fig. 9C). The first-order reaction rate constant increases as increasing the temperature from 278 to 308 K, then decreases a little at 323 K (inset of Fig. 9C). Two main factors may be responsible for this trend, the content of the dissolved oxygen and the collision probability between radicals and U(VI). The former decreases with the increase of the temperature [60], but the latter is the opposite. Under the influence of these two factors, the elimination of U(VI) in solution reaches a maximum at 308 K. The ultrasonic power (Fig. 9D and its inset) is another factor that may have a great influence on the elimination of U(VI). It is interesting to find an optimal power is at 120 W. Generally, the high ultrasonic power is favorable for the generation of H_2O_2, but too high ultrasonic power may lead to the escape of soluble oxygen due to the strong vibration of the water. The frequency-dependent U(VI) removal is also performed and shown in Fig. 9E and its inset, from which the piezo catalytic activity steadily increases with increasing the ultrasonic frequencies from 28 to 50 kHz at a fixed power of 50 W. All the solids after piezo catalysis are collected and analyzed by XRD, which clearly disclose the formation of $(UO_2)O_2.2H_2O$(s) (Figs. S9(A-D)). Besides, the characteristic peak intensities of $(UO_2)O_2.2H_2O$(s) are highly positively correlated with the catalytic efficiency as shown in Figs. S9(B-D).

The effects of various cations and anions (K^+, Na^+, Mg^{2+}, NO_3^-, SO_4^{2-}, CO_3^{2-}, and PO_4^{3-}) with a concentration of 0.05 mol/L on U(VI) removal are investigated and shown in Fig. 9F and its inset. Specifically, K^+ has a strong suppressing effect on the piezo catalytic removal of U (VI), while that of Na^+ and Mg^{2+} are relatively weak. The different inhibiting effects can be explained by the ionic specificities of these introduced cations. It is proposed that K^+ is a chaotropic ion with weakly-held hydration shells and has weak interactions with water molecules, while Na^+ and Mg^{2+} are kosmotropic ions with strongly-held hydration shells and have stable interactions with water molecules [61]. Therefore, the weakly hydrated K^+ is easier to lose the hydration layers and approaches the surfaces of the catalyst as a free ion. The concentration of K^+ (0.05 M) is over 200 times higher than U(VI) (50 ppm, 0.00021 M). The excessive K^+ occupies the surface-active sites of catalyst and suppresses the adsorption and catalysis of U(VI). Whereas Na^+ and Mg^{2+} exist as stable hydrated ions in solution and are hardly seized by the catalyst, the obstruction is thus weak. However, the influences of anions on the catalytic process are much more complicated. The effect of NO_3^- toward U(VI) removal can be almost ignored. SO_4^{2-} has a negative effect on both the adsorption and piezo catalytic removal of U(VI) due to

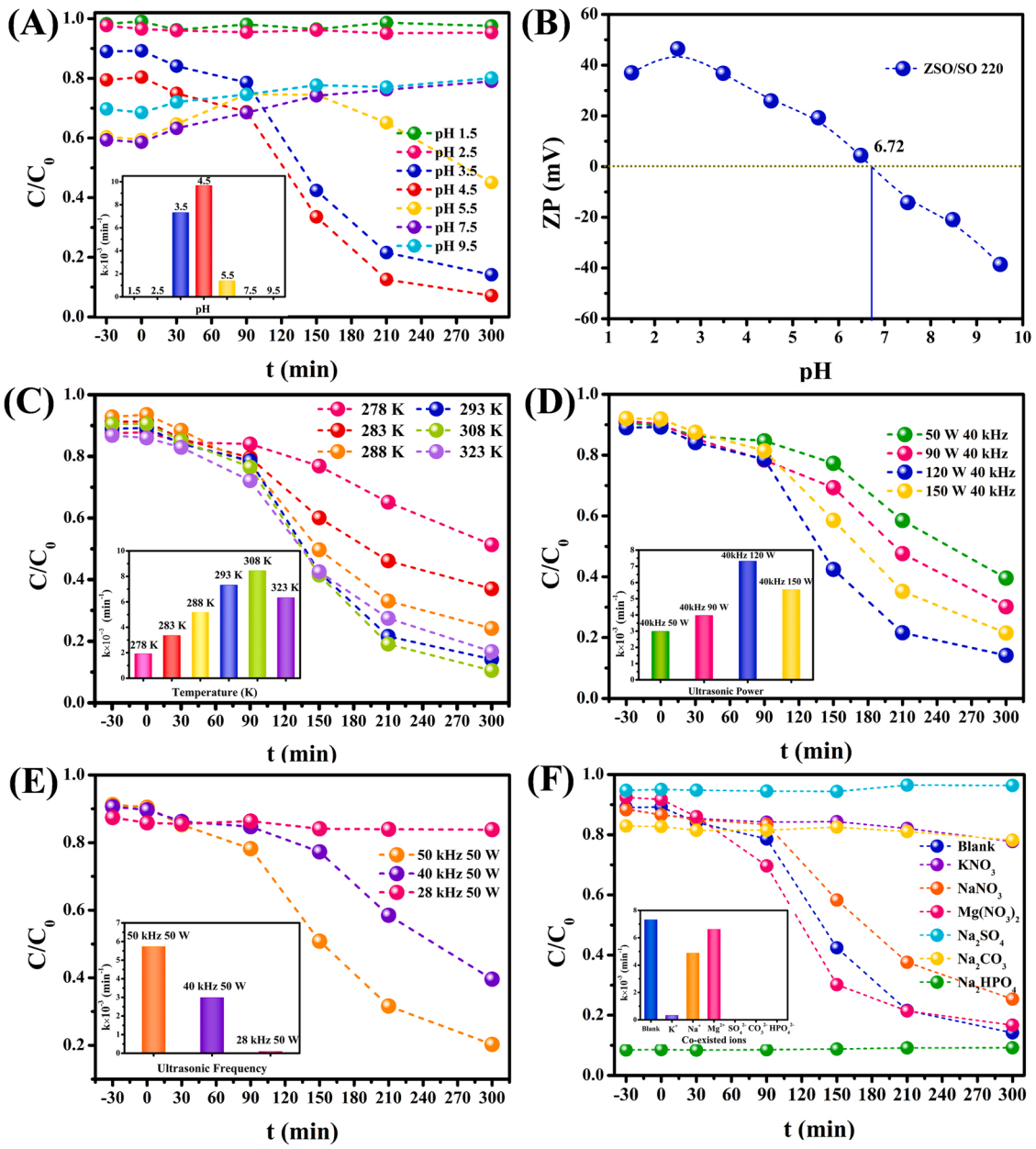

Fig. 9. . (A) Piezo catalytic U(VI) removal rate and the corresponding fitted results of the removal rate constant (inset) by using ZSO/SO 220 under different solution pH. m/V= 1.0 g/L, $C_{U(VI)\ initial}$= 50 mg/L, T = 293 K; (B) Zeta potentials of ZSO/SO 220 ranges from pH 1.5–9.5. m/V= 1.0 g/L, T = 293 K; Piezo catalytic U(VI) removal rate and the corresponding fitted results of the removal rate constant (inset) by using ZSO/SO 220 under different (C) temperatures, (D) powers, and (E) frequencies of ultrasonic waves. m/V= 1.0 g/L, $C_{U(VI)\ initial}$= 50 mg/L, pH= 3.50 ± 0.02; (F) Effects of different cations and anions on piezo catalytic removal of U (VI) and the corresponding fitted results of the removal rate constant (inset), m/V= 1.0 g/L, $C_{U(VI)\ initial}$= 50 mg/L, pH= 3.50 ± 0.02, T = 293 K. For convenient comparison, the blue curve in (A) was re-drawn in (C), (D), and (F).

the existence of more than 60% of soluble UO_2SO_4(aq) and ~30% of $UO_2(SO_4)_2^{2-}$ in the reaction system (Fig. S10). Usually, CO_3^{2-} can form stable complexes with U(VI) (such as UO_2CO_3(aq) and $UO_2(CO_3)_2^{2-}$) in solution and thus decrease the removal of U(VI). The added PO_4^{3-} has a positive impact on the adsorption process as almost all the U(VI) in solution is eliminated during the adsorption/desorption equilibrium by forming the precipitation of UO_2HPO_4(s).

3.6. *Recycling performance*

To evaluate the stability and reusability of ZSO/SO 220, the piezo catalytic experiment was performed consecutively repeated four cycles of extraction-regeneration. The extracted uranium on ZSO/SO 220 can be almost completely eluted by 0.1 M Na_2CO_3 under 1.5 h stirring and 5 min ultrasound assistant. The results are shown in Fig. 10, from which the extraction of uranium slightly decreased from ~85% to ~82% after four cycles, indicating the excellent regeneration and recycling properties of the catalyst.

4. Conclusions

In summary, soluble U(VI) ions are successfully extracted by piezo catalytic technique, which is immobilized to form $(UO_2)O_2$•2 H_2O(s) on the surface of a novel hollow nanocubes of ZSO/SO. The piezo catalytic process is confirmed to be controlled by a three-step process, adsorption, reduction, and oxidation by systematically investigating and analyzing

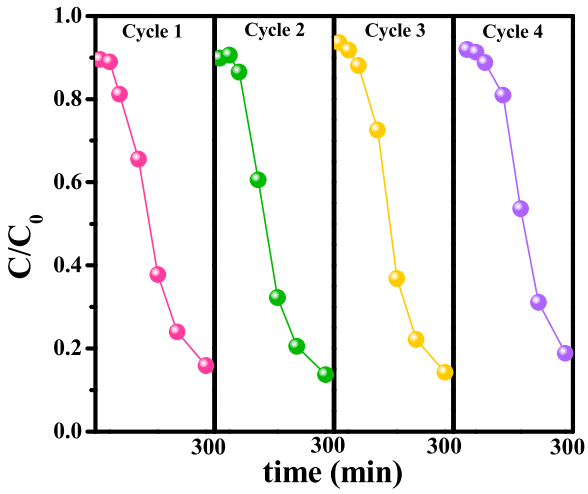

Fig. 10. Recyclability and recovery study of ZSO/SO 220 for U(VI) extraction.

the piezo catalytic experiments, which exhibits a reverse *S* shape in the piezo catalytic kinetic curve. The U(VI) is firstly adsorbed onto the surfaces of ZSO/SO nanocomposite, and then is reduced by the piezo generated electrons to form UO_2(s). Interestingly, the piezo generated electrons also react with dissolved oxygen to produce the oxidizer H_2O_2 and this active oxygen species can re-oxidize the UO_2(s) to (UO_2)O_2•$2H_2O$(s). Additionally, the piezo induced electrons and holes are efficiently separated due to the type II matching of the bandgap of ZSO and SO, thereby generating more available radicals in U(VI) piezo catalytic extraction. Thus, this work realizes the innovative application of piezo catalysis in the field of U(VI) extraction from solution and provides an in-depth insight into piezo catalytic mechanisms between the catalyst and heavy metals, and has great value in the collection and treatment of U(VI) containing water.

CRediT authorship contribution statement

Yawen Cai: Methodology, Formal analysis, Investigation, Data curation, Software, Validation, Writing – original draft. **Yifeng Zhang**: Software and Methodology. **Zhimin Lv**: Formal analysis and Data curation. **Shuo Zhang**: Data curation and Validation. **Feixue Gao**: Data curation and Validation. **Ming Fang**: Conceptualization, Discussion, Writing – review & editing, Supervision, Funding acquisition, Project administration. **Mingguang Kong**: Investigation. **Peisheng Liu**: Validation. **Xiaoli Tan**: Writing – review & editing, Supervision, Funding acquisition. **Baowei Hu**: Investigation, review. **Xiangke Wang**: Validation, Writing – review & editing, Supervision, Funding acquisition.

Declaration of Competing Interest

The authors declear that there is no conflict-of-interest.

Acknowledgments

Financial supports from National Natural Science Foundation of China (21876047), National Key Research and Development Program of China (2018YFC1900105), Science Challenge Project (TZ2016004), the Beijing Outstanding Young Scientist Program and the Thousand Talents Plan of Qinghai province.

Appendix A. Supporting information

Supplementary data associated with this article can be found in the online version at doi:10.1016/j.apcatb.2022.121343.

References

[1] I. Tabushi, Y. Kobuke, T. Nishiya, Extraction of uranium from seawater by polymer-bound macrocyclic hexaketone, Nature 280 (1979) 665–666.
[2] C. Liu, P.-C. Hsu, J. Xie, J. Zhao, T. Wu, H. Wang, W. Liu, J. Zhang, S. Chu, Y. Cui, A half-wave rectified alternating current electrochemical method for uranium extraction from seawater, Nat. Energy 2 (2017) 17007.
[3] S.J. Morrison, D.R. Metzler, C.E. Carpenter, Uranium precipitation in a permeable reactive barrier by progressive irreversible dissolution of zerovalent iron, Environ. Sci. Technol. 35 (2001) 385–390.
[4] J.R. Kumar, J.-S. Kim, J.-Y. Lee, H.-S. Yoo, A brief review on solvent extraction of uranium from acidic solutions, Sep. Purif. Rev. 40 (2011) 77–125.
[5] Y. Cai, Y. Ma, J. Feng, M. Zhu, X. Wang, Z. Lv, M. Fang, X. Tan, X. Wang, Insight into the performance and mechanism of low-cost phytic acid modified Zn-Al-Ti LMO for U(VI) removal, Chem. Eng. J. 402 (2020), 125510.
[6] G. Cheng, A. Zhang, Z. Zhao, Z. Chai, B. Hu, B. Han, Y. Ai, X. Wang, Extremely stable amidoxime functionalized covalent organic frameworks for uranium extraction from seawater with high efficiency and selectivity, Sci. Bull. 66 (2021) 1996–2001.
[7] H. Deng, Z. Li, L. Wang, L. Yuan, J. Lan, Z. Chang, Z. Chai, W. Shi, Nanolayered Ti3C2 and SrTiO3 composites for photocatalytic reduction and removal of uranium (VI), ACS Appl. Nano Mater. 2 (2019) 2283–2294.
[8] S. Li, Y. Hu, Z. Shen, Y. Cai, Z. Ji, X. Tan, Z. Liu, G. Zhao, S. Hu, X. Wang, Rapid and selective uranium extraction from aqueous solution under visible light in the absence of solid photocatalyst, Sci. China Chem. 64 (2021) 1323–1331.
[9] H. Yang, X. Liu, M. Hao, Y. Xie, X. Wang, H. Tian, G.I.N. Waterhouse, P.E. Kruge, S. G. Telfer, S. Ma, Functionalized iron–nitrogen–carbon electrocatalyst provides a reversible electron transfer platform for efficient uranium extraction from seawater, Adv. Mater. (2021), 2106621.
[10] J.M. Wu, W.E. Chang, Y.T. Chang, C.-K. Chang, Piezo-catalytic effect on the enhancement of the ultra-high degradation activity in the dark by single- and few-layers MoS_2 nanoflowers, Adv. Mater. 28 (2016) 3718–3725.
[11] S. Tu, Y. Guo, Y. Zhang, C. Hu, T. Zhang, T. Ma, H. Huang, Piezocatalysis and piezo-photocatalysis: catalysts classification and modification strategy, reaction mechanism, and practical application, Adv. Funct. Mater. 30 (2020), 2005158.
[12] H. You, Z. Wu, L. Zhang, Y. Ying, Y. Liu, L. Fei, X. Chen, Y. Jia, Y. Wang, F. Wang, S. Ju, J. Qiao, C.-H. Lam, H. Huang, Harvesting the vibration energy of $BiFeO_3$ nanosheets for hydrogen evolution, Angew. Chem. 131 (2019) 11905–11910.
[13] J. Wu, N. Qin, D. Bao, Effective enhancement of piezocatalytic activity of $BaTiO_3$ nanowires under ultrasonic vibration, Nano Energy 45 (2018) 44–51.
[14] Q. Zhao, H. Xiao, G. Huangfu, Z. Zheng, J. Wang, F. Wang, Y. Guo, Highly-efficient piezocatalytic performance of nanocrystalline $BaTi_{0.89}Sn_{0.11}O_3$ catalyst with Tc near room temperature, Nano Energy 85 (2021), 106028.
[15] A. Zhang, Z. Liu, B. Xie, J. Lu, K. Guo, S. Ke, L. Shu, H. Fan, Vibration catalysis of eco-friendly $Na_{0.5}K_{0.5}NbO_3$-based piezoelectric: an efficient phase boundary catalyst, Appl. Catal. B: Environ. 279 (2020), 119353.
[16] S. Li, Z. Zhao, D. Yu, J.-Z. Zhao, Y. Su, Y. Liu, Y. Lin, W. Liu, H. Xu, Z. Zhang, Few-layer transition metal dichalcogenides (MoS_2, WS_2, and WSe_2) for water splitting and degradation of organic pollutants: understanding the piezocatalytic effect, Nano Energy 66 (2019), 104083.
[17] Y. Sun, X. Li, A. Vijayakumar, H. Liu, C. Wang, S. Zhang, Z. Fu, Y. Lu, Z. Cheng, Hydrogen generation and degradation of organic dyes by new piezocatalytic $0.7BiFeO_3$-$0.3BaTiO_3$ nanoparticles with proper band alignment, ACS Appl. Mater. Interfaces 13 (2021) 11050–11057.
[18] D. Liu, Y. Song, Z. Xin, G. Liu, C. Jin, F. Shan, High-piezocatalytic performance of eco-friendly $(Bi_{1/2}Na_{1/2})TiO_3$-based nanofibers by electrospinning, Nano Energy 65 (2019), 104024.
[19] M. Pan, S. Liu, J.W. Chew, Unlocking the high redox activity of MoS_2 on dual-doped graphene as a superior piezocatalyst, Nano Energy 68 (2020), 104366.
[20] S. Lan, J. Feng, Y. Xiong, S. Tian, S. Liu, L. Kong, Performance and mechanism of piezo-catalytic degradation of 4-chlorophenol: finding of effective piezo-dechlorination, Environ. Sci. Technol. 51 (2017) 6560–6569.
[21] Y. Wei, Y. Zhang, W. Geng, H. Su, M. Long, Efficient bifunctional piezocatalysis of $Au/BiVO_4$ for simultaneous removal of 4-chlorophenol and Cr(VI) in water, Appl. Catal. B: Environ. 259 (2019), 118084.
[22] W. Tian, J. Qiu, N. Li, D. Chen, Q. Xu, H. Li, J. He, J. Lu, Efficient piezocatalytic removal of BPA and Cr(VI) with SnS_2/CNFs membrane by harvesting vibration energy, Nano Energy 86 (2021), 106036.
[23] S. Sun, S. Liang, Morphological zinc stannate: synthesis, fundamental properties and applications, J. Mater. Chem. A 5 (2017) 20534–20560.
[24] Y. Zhang, M. Zhu, S. Zhang, Y. Cai, Z. Lv, M. Fang, X. Tan, X. Wang, Highly efficient removal of U(VI) by the photoreduction of SnO_2/$CdCO_3$/CdS nanocomposite under visible light irradiation, Appl. Catal. B: Environ. 279 (2020), 119390.
[25] T.P. Yendrapati, A. Gautam, S. Bojja, U. Pal, Formation of ZnO@CuS nanorods for efficient photocatalytic hydrogen generation, Sol. Energy 196 (2020) 540–548.
[26] J. Zhang, J. Lang, Y. Wei, Q. Zheng, L. Liu, Y.-H. Hu, B. Zhou, C. Yuan, M. Long, Efficient photocatalytic H_2O_2 production from oxygen and pure water over graphitic carbon nitride decorated by oxidative red phosphorus, Appl. Catal. B: Environ. 298 (2021), 120522.
[27] H. Yu, H. Huang, A.H. Reshak, S. Auluck, L. Liu, T. Ma, Y. Zhang, Coupling ferroelectric polarization and anisotropic charge migration for enhanced CO_2 photoreduction, Appl. Catal. B: Environ. 284 (2021), 119709.
[28] H. Qi, A. Xie, A. Tian, R. Zuo, Superior energy-storage capacitors with simultaneously giant energy density and efficiency using nanodomain engineered $BiFeO_3$-$BaTiO_3$-$NaNbO_3$ lead-free bulk ferroelectrics, Adv. Energy Mater. 10 (2019), 1903338.

[29] V. Bhavanasi, D.Y. Kusuma, P.S. Lee, Polarization orientation, piezoelectricity, and energy harvesting performance of ferroelectric PVDF-TrFE nanotubes synthesized by nanoconfinement, Adv. Energy Mater. 4 (2014), 1400723.
[30] P. Wang, X. Li, S. Fan, X. Chen, M. Qin, D. Long, M.O. Tadé, S. Liu, Impact of oxygen vacancy occupancy on piezo-catalytic activity of $BaTiO_3$ nanobelt, Appl. Catal. B: Environ. 279 (2020), 119340.
[31] R. Su, Z. Wang, L. Zhu, Y. Pan, D. Zhang, H. Wen, Z.-D. Luo, L. Li, F.-t Li, M. Wu, L. He, P. Sharma, J. Seidel, Strain-engineered nano-ferroelectrics for high-efficiency piezocatalytic overall water splitting, Angew. Chem. 133 (2021) 16155–16162.
[32] X. Huang, R. Lei, J. Yuan, F. Gao, C. Jiang, W. Feng, J. Zhuang, P. Liu, Insight into the piezo-photo coupling effect of $PbTiO_3$/CdS composites for piezo-photocatalytic hydrogen production, Appl. Catal. B: Environ. 282 (2021), 119586.
[33] T. Xiong, Q. Li, J. Liao, Y. Zhang, W. Zhu, Highly enhanced adsorption performance to uranium(VI) by facile synthesized hydroxyapatite aerogel, J. Hazard. Mater. 423 (2022), 127184.
[34] H. Wang, H. Guo, N. Zhang, Z. Chen, B. Hu, X. Wang, Enhanced photoreduction of U(VI) on C3N4 by Cr(VI) and bisphenol A: ESR, XPS and EXAFS investigation, Environ. Sci. Technol. 53 (2019) 6454–6461.
[35] S. Liu, Z. Wang, Y. Lu, H. Li, X. Chen, G. Wei, T. Wu, D.-J. Maguire, G. Ye, J. Chen, Sunlight-induced uranium extraction with triazine-based carbon nitride as both photocatalyst and adsorbent, Appl. Catal. B: Environ. 282 (2021), 119523.
[36] T. Sato, Thermal decomposition of uranium peroxide hydrates, J. Appl. Chem. Biorechnol. 26 (1976) 207–213.
[37] T.B. Scott, G.C. Allen, P.J. Heard, M.G. Randell, Reduction of U (VI) to U (IV) on the surface of magnetite, Geochim. Cosmochim. Acta 69 (2005) 5639–5646.
[38] M.D. Straub, J. Leduc, M. Frank, A. Raauf, T.D. Lohrey, S.G. Minasian, S. Mathur, J. Arnold, Chemical vapor deposition of phase-pure uranium dioxide thin films from uranium(IV) amidate precursors, Angew. Chem. Int. Ed. 58 (2019) 5749–5753.
[39] Z. Chen, X. He, Q. Li, H. Yang, Y. Liu, L. Wu, Z. Liu, B. Hu, X. Wang, Low-temperature plasma induced phosphate groups onto coffee residue-derived porous carbon for efficient U(VI) extraction, J. Environ. Sci. 122 (2022) 1–13.
[40] S. Wang, L. Shi, S. Yu, H. Pang, M. Qiu, G. Song, D. Fu, B. Hu, X. Wang, Effect of shewanella oneidensis MR-1 on U(VI) sequestration by montmorillonite, J. Environ. Radioact. 242 (2022), 106798.
[41] M.R. Hoffmann, S.T. Martin, W. Choi, D.W. Bahnemann, Environmental applications of semiconductor photocatalysis, Chem. Rev. 95 (1995) 69–96.
[42] Y.-C. Wang, J.M. Wu, Effect of controlled oxygen vacancy on H_2-production through the piezocatalysis and piezophototronics of ferroelectric R3C $ZnSnO_3$ nanowires, Adv. Funct. Mater. 30 (2020), 1907619.
[43] S. Lan, X. Zeng, R.A. Rathera, I.M.C. Lo, Enhanced trimethoxypyrimidine degradation by piezophotocatalysis of $BaTiO_3/Ag_3PO_4$ using mechanical vibration and visible light simultaneously, Environ. Sci. Nano 6 (2019) 554–564.
[44] S. Dursun, H. Akyildiz, V. Kalem, PMN-PT nanoparticle/SnO_2 nanofiber heterostructures: Enhanced photocatalytic degradation performance by ultrasonic wave induced piezoelectric field, J. Alloy. Compd. 889 (2021), 161769.
[45] F. Mohamadkhani, S. Javadpour, N. Taghavini, Improvement of planar perovskite solar cells by using solution processed SnO_2/CdS as electron transport layer, Sol. Energy 191 (2019) 647–653.
[46] H. Tsuchiya, S. Fujimoto, O. Chihara, T. Shibata, Semiconductive behavior of passive films formed on pure Cr and Fe-Cr alloys in sulfuric acid solution, Electrochim. Acta 47 (2002) 4357–4366.
[47] F. Guo, W. Shi, H. Wang, M. Han, H. Li, H. Huang, Y. Liu, Z. Kang, Facile fabrication of a CoO/g-C_3N_4 p-n heterojunction with enhanced photocatalytic activity and stability for tetracycline degradation under visible light, Catal. Sci. Technol. 7 (2017) 3325–3331.
[48] C. Corbel, G. Sattonnay, S. Guilbert, F. Garrido, M.-F. Barthe, C. Jegou, Addition versus radiolytic production effects of hydrogen peroxide on aqueous corrosion of UO_2, J. Nucl. Mater. 348 (2006) 1–17.
[49] M. Amme, W. Bors, C. Michel, K. Stettmaier, G. Rasmussen, M. Betti, Effects of Fe (II) and hydrogen peroxide interaction upon dissolving UO_2 under geologic repository conditions, Environ. Sci. Technol. 39 (2005) 221–229.
[50] R.J. Wilbraham, C. Boxall, D.T. Goddard, R.J. Taylor, S.E. Woodbury, The effect of hydrogen peroxide on uranium oxide films on 316L stainless steel, J. Nucl. Mater. 464 (2015) 86–96.
[51] K.-A.H. Kubatko, K.B. Helean, A. Navrotsky, P.C. Burns, Stability of peroxide-containing uranyl minerals, Science 302 (2003) 1191–1193.
[52] S. Hickam, J. Breier, Y. Cripe, E. Cole, P.C. Burns, Effects of H_2O_2 concentration on formation of uranyl peroxide species probed by dissolution of uranium nitride and uranium dioxide, Inorg. Chem. 58 (2019) 5858–5864.
[53] E.L. Bright, S. Rennie, A. Siberry, K. Samani, K. Clarke, D.T. Goddard, R. Springell, Comparing the corrosion of uranium nitride and uranium dioxide surfaces with H_2O_2, J. Nucl. Mater. 518 (2019) 202–207.
[54] Y. Lei, S. Xu, M. Ding, L. Li, Q. Sun, Z.L. Wang, Enhanced photocatalysis by synergistic piezotronic effect and exciton-plasmon interaction based on (Ag-Ag_2S)/$BaTiO_3$ heterostructures, Adv. Funct. Mater. 30 (2020), 2005716.
[55] Z. Zhang, Y. Liang, H. Huang, X. Liu, Q. Li, L. Chen, D. Xu, Stable and highly efficient photocatalysis with lead-free double-perovskite of $Cs_2AgBiBr_6$, Angew. Chem. Int. Ed. 58 (2019) 7263–7267.
[56] X. Guo, S.V. Ushakov, S. Labs, H. Curtius, D. Bosbach, A. Navrotsky, Energetics of metastudtite and implications for nuclear waste alteration, P. Natl. Acad. Sci. USA 111 (2014) 17737–17742.
[57] R.J. Finchi, M.A. Coopera, F.C. Hawthorne, The crystal structure of schoepite, $[(UO_2)_8O_2(OH)_{12}](H_2O)_{12}$, Can. Mineral. 34 (1996) 1071–1088.
[58] O.V. Nipruk, A.V. Knyazev, G.N. Chernorukov, Yu.P. Pykhova, Synthesis and study of hydrated uranium(VI) oxides, $UO_3{\cdot}nH_2O$, Radiochemistry 53 (2011) 146–150.
[59] A.G. Sowder, S.B. Clark, R.A. Fjeld, The transformation of uranyl oxide hydrates: the effect of dehydration on synthetic metaschoepite and its alteration to becquerelite, Environ. Sci. Technol. 33 (1999) 3552–3557.
[60] D.J. Graczyk, W.C. Sonzogni, Reduction of dissolved oxygen concentration in wisconsin streams during summer runoff, J. Environ. Qual. 20 (1991) 445–451.
[61] K.C. Kang, P. Linga, K.N. Park, S.J. Choi, J.D. Lee, Seawater desalination by gas hydrate process and removal characteristics of dissolved ions (Na^+, K^+, Mg^{2+}, Ca^{2+}, B^{3+}, Cl^-, SO_4^{2-}), Desalination 353 (2014) 84–90.